Journal of Solid State Chemistry **168,** 497–502 (2002)
doi:10.1006/jssc.2002.9734

Optical Study of Two-Dimensional Organic Metal $(EO\text{-}TTP)_2AsF_6$ (EO-TTP=2-(4,5-Ethylenedioxy-1,3-Dithiol-2-Ylidene)-5-(1,3-Dithiol-2-Ylidene)-1,3,4,6-Tetrathiapentalene)

O. Drozdova,*,[1] K. Yakushi,*,[2] Y. Misaki,† and K. Tanaka†

*Institute for Molecular Science, University of Tokyo, Nishigonaka 38, Myodaiji, Okazaki, Aichi, 444-8585 Japan; and †Department of Molecular Engineering, Kyoto University, Kyoto 606-8501, Japan

Received January 7, 2002; in revised form March 11, 2002; accepted April 10, 2002

Polarized reflectance spectra were measured on the conductive (010) plane of metallic $(EO\text{-}TTP)_2AsF_6$ single crystal. At room temperature, well-defined plasma edges appeared in both directions parallel ($E||a$) and perpendicular ($E\perp a$) to the molecular stack. The intra- and inter-stack transfer integrals were estimated from the plasma frequencies in the framework of tight-binding model. Based on these transfer integrals, we suggested that the Fermi surface was open in the k_c direction. Using a generalized Drude model, we obtained the frequency dependence of relaxation rate, which conformed to $\gamma(\omega) = \gamma_0 + b\omega^2$ in the frequency range 1800–5500 cm^{-1}. © 2002 Elsevier Science (USA)

Key Words: **tetrathia pentalene; estimation of transfer integrals; two-dimensional organic metal; frequency dependence of relaxation rate; polarized reflection spectrum.**

1. INTRODUCTION

2,5-Bis(1,3-dithiol-2-ylidene)-1,3,4,6-tetrathiapentalene BDT-TTP and its derivatives including TTP skeleton have been found to give enormous number of metallic charge-transfer salts down to liquid helium temperature (1–8). EO-TTP (2-(4,5-ethylenedioxy-1,3-dithiol-2-ylidene)- 5-(1,3-dithiol-2-ylidene)-1,3,4,6-tetrathiapentalene) belongs to the metallic BDT-TTP family with an asymmetric structure, in which ethylenedioxy group is substituted at one of the five member rings (see the inset of Fig. 2). Misaki *et al*. present the temperature dependence of the resistivity and thermopower of $(EO\text{-}TTP)_2AsF_6$ (9). The resistivity and thermopower show metallic behavior down to 1.5 K. The stable metallic property is regarded as the result of the small on-site Coulomb energy due to the extended π-electron molecular orbital and the strong inter-chain interaction through short side-by-side S–S contacts. To get the knowledge on the dimensionality of this compound, Misaki *et al*. calculated the overlap integrals between the HOMOs (highest-occupied molecular orbital) of neighbor molecules, and present the tight-binding band with a closed Fermi surface (9). However, there is no experimental evidence to support the closed Fermi surface and small on-site Coulomb energy for this compound. The purpose of this paper is the characterization of the electronic structure of this metallic compound through the analysis of the reflectivity. First, we evaluate the intra- and inter-stack transfer integrals using the same method as Ref. (10). Second, we examine the frequency dependence of the relaxation rate using a generalized Drude model to obtain the information on the electron–electron interaction.

2. EXPERIMENTAL

Single crystals of $(EO\text{-}TTP)_2AsF_6$ were prepared by electrochemical method described in Ref. (9). The polarized reflection spectrum in the NIR and visible region was measured on an Atago Multiviewer spectrometer with multi-channel detection system combined with a SPECTRA TECH IR-Plan microscope. The same microscope was combined with FT-IR, Nicolet Magna 750 for the measurement of NIR and IR regions. The details of the experimental apparatus including cryostat system were described elsewhere (10). The sample size for the low-temperature experiment was ca. $1 \times 0.2 \times 0.1\,mm^3$. The reflectivity was measured on the most developed crystal face (010) with polarizations of maximum and minimum reflectivities in the infrared region. The maximum

[1] Permananent address: Ioffe Physico-Technical Institute, Russian Academy of Sciences, 194022 St. Petersburg, Russia. Present address: Department of Physics, University of Florida, PO Box 118440, Ganesville, Florida 32611-8440.

[2] To whom correspondence should be addressed. E-mail: yakushi@ims.ac.jp.

0022-4596/02 $35.00

reflectivity was observed when the light polarization was parallel to the *a*-axis (needle axis).

3. RESULTS AND DISCUSSION

3.1. Evaluation of the Dimensionality

The crystal of $(EO\text{-}TTP)_2AsF_6$ belongs to the triclinic system with the space group of $P\bar{1}$ (9), which is isostructural to that of $(BDT\text{-}TTP)_2SbF_6$ (1). The EO-TTP molecules are stacked along the *a*-axis aligning the long molecular axis nearly along the [112] direction. The EO-TTP molecules form a conducting sheet in the (010) plane, which is separated from the neighbor sheet by counter anions. The conducting sheet viewed along the long molecular axis is drawn in Fig. 1 along with the definition of the transfer integrals between the neighbor molecules. The unit cell contains two molecules (A and A′), which are connected by inversion symmetry, so the overlap modes A-A′ and A′-A are crystallographically non-equivalent. Reflecting this structure, the transfer integrals (t_{a1} and t_{a2}) along the *a*-axis are non-uniform. However, it is expected from the calculation of overlap integrals that t_{a1} and t_{a2} are nearly equal to each other, that is, the dimerization in the molecular stack is very weak (9).

Figure 2 shows the reflection spectra measured with polarizations parallel ($E||a$) and perpendicular ($E\perp a$) to the stacking direction on the (010) crystal face. Strong metallic dispersions appear in both directions in the infrared region. To obtain quantitative information on the dimensionality, we conducted Drude analysis. Since the plasma frequency is strongly correlated with the dielectric constant ε_∞ in the Drude analysis, we applied Drude model for the low-frequency region and Lorentz model for the high-frequency region to avoid the influence on the dielectric constant from the inter-band transition. The best-fit curves are drawn by dotted lines in the same figure. In contrast to $(TMTSF)_2PF_6$ (11, 12) and β-$(BEDT\text{-}TTF)_2I_3$ (13), the low-frequency reflectivity is fitted well down to $750\,cm^{-1}$ by Drude model. Table 1 gives the Drude parameters and hole effective masses m_i^*/m_e which are calculated by the relation $(\omega_{pi})^2 = ne^2/\varepsilon_0 m_i^*$ where n is the hole density, ε_0 the dielectric constant of vacuum, i the direction of the polarization of light, and m_e the electron mass. For a more quantitative comparison with the theoretical calculation, the plasma frequency was calculated using the following equation (13):

$$\omega_p^2(i) = \frac{ne^2}{\varepsilon_0\hbar^2}\frac{\iint f(E(k_ak_c))(\partial^2 E(k_ak_c)/\partial k_i^2)dk_a dk_c}{\iint f(E(k_ak_c))\,\mathrm{d}k_a\,\mathrm{d}k_c}, \quad [1]$$

where $E(k_a, k_c)$ is the two-dimensional energy dispersion, $f(E)$ the Fermi-Dirac function, and i denotes the polarization directions $E||a$ and $E\perp a$ on the (010) plane. We divided the first Brillouin zone into 200×200 meshes, and numerically integrated the second derivatives of $E(k_a, k_c)$ assuming $T = 0$ K for the distribution function. Misaki *et al.* present the overlap integrals (S) in $(EO\text{-}TTP)_2AsF_6$ (9) Assuming the empirical relation $t = -10S$ eV, we tentatively estimated the transfer integrals as $t_{a1} = -0.269$, $t_{a2} = -0.252$, $t_c = 0.0907$, $t_{p1} = -0.0047$, and $t_{p2} = -0.0011$ eV. The two-dimensional energy dispersion $E(k_a, k_c)$ is expressed by the following equation:

$$E(k_a, k_c) = 2t_c\cos(k_c c) \pm |H_{12}|, \quad [2]$$

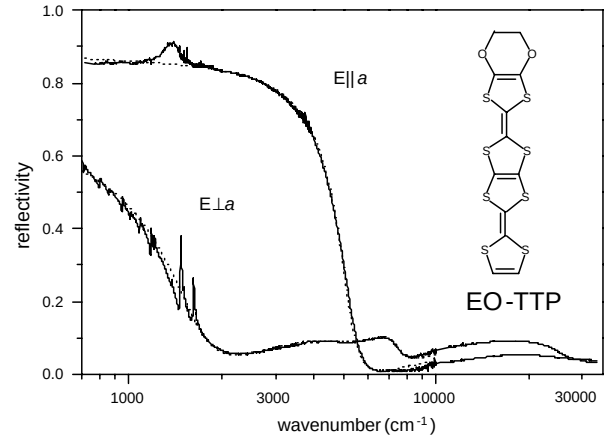

FIG. 2. Polarized reflection spectra with the polarizations of $E||a$ and $E\perp a$ measured at room temperature. The dotted lines show the reflectivity calculated using Drude–Lorentz model.

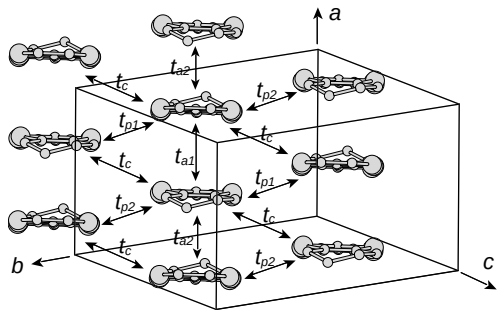

FIG. 1. Molecular arrangement in the conducting sheet viewed along the long molecular axis and the definition of the transfer integrals.

TABLE 1
Drude Parameters at 300 K

	ε_∞	γ (cm^{-1})	ω_p^{obs}	m^*/m_e	ω_p^{calc} (cm^{-1})
$E\|\|a$	2.5	680	8990	1.3	9360
$E\perp a$	3.1	900	3450	8.6	6510

and

$$H_{12}^2 = t_{a1}^2 + t_{a2}^2 + t_{p1}^2 + t_{p2}^2 + 2t_{a1}t_{a2}\cos(k_a a) + 2(t_{a1}t_{p1} + t_{a2}t_{p2})\cos(k_c c) + 2(t_{a1}t_{p2} + t_{a2}t_{p1})\cos(k_a a + k_c c) + 2t_{p1}t_{p2}\cos(k_a a + 2k_c c),$$

where a and c are the lattice constants, k_a and k_c are the reciprocal vector running in the first Brillouin zone. The plasma frequencies are calculated using Eqs. (1) and (2). The results are given in the last column of Table 1. The anisotropic ratio of the plasma frequency $\omega_p^{calc}(E\perp a)/\omega_p^{calc}(E||a)$ is almost twice as large as the experimental value. We estimate the intra- and inter-stack transfer integrals to reproduce the observed plasma frequencies using the approximation described below. According to the calculation of the overlap integrals (9), t_{a1} is nearly equal to t_{a2}, and t_{p1} and t_{p2} are more than an order of magnitude smaller compared with t_a and t_c. Hence, we take an approximation as $t_{a1}=t_{a2}=t_a$, $t_{p1}=t_{p2}=0$. Under this approximation, $E(k_a, k_c)$ is expressed only by two parameters t_a and t_c. To obtain t_a and t_c, we numerically solved the simultaneous equations (1) for $\omega_p(E||a)$ and $\omega_p(E\perp a)$ by dividing the first Brillouin zone into 200×200 meshes. The best solution is the set of $|t_a|=0.23$ eV and $|t_c|=0.047$ eV, which gives $\omega_p(E||a)=9.00\times10^3\,\mathrm{cm}^{-1}$ and $\omega_p(E\perp a)=3.45\times10^3\,\mathrm{cm}^{-1}$. We therefore conclude that the theoretical calculation overestimates the overlap integral corresponding to t_c, or underestimates that corresponding to t_a.

Figure 3 shows the comparison of the energy dispersions and Fermi surfaces, which are calculated using the experimentally obtained and theoretically estimated transfer integrals (14). The most different point is the shape of the Fermi surface. The theoretical calculation predicts a

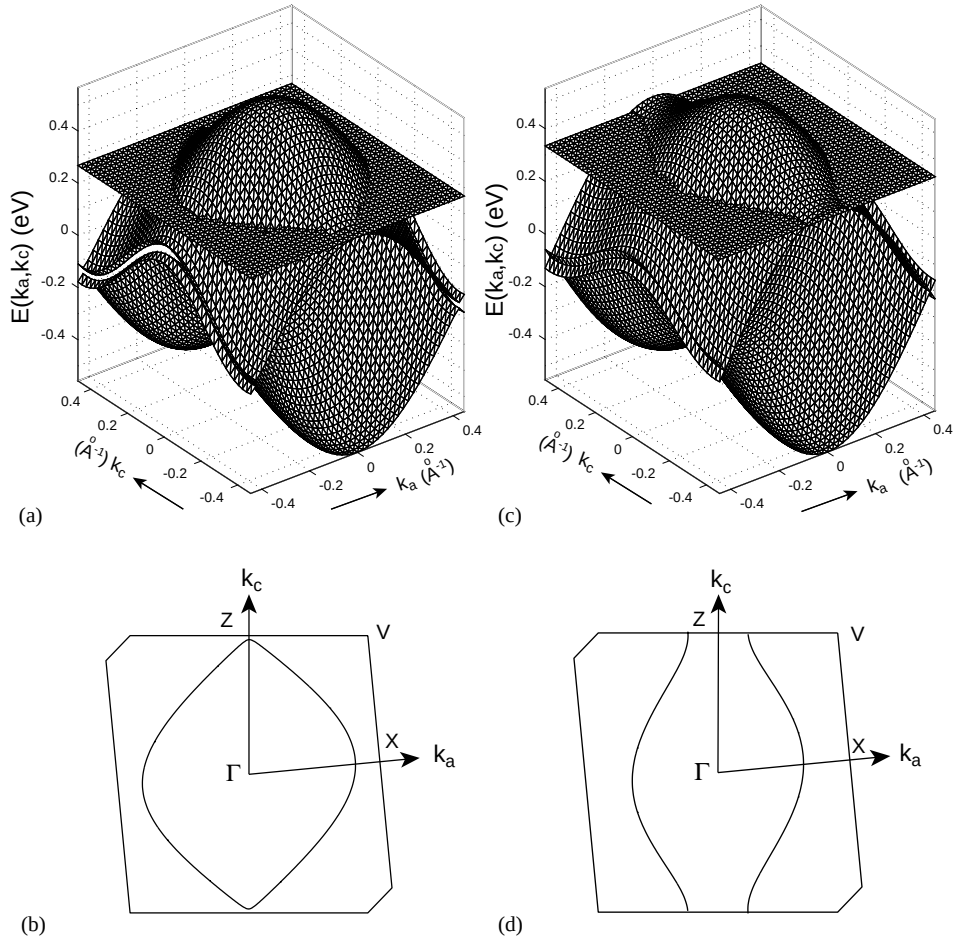

FIG. 3. Energy dispersion $E(k_a, k_c)$ in a reciprocal cell and Fermi surface in a Wigner–Seitz cell: (a) $E(k_a, k_c)$ and (b) Fermi surface calculated using the theoretically calculated transfer integrals; (c) $E(k_a, k_c)$ and (d) Fermi surface calculated using the experimentally obtained transfer integrals. $E(k_a, k_c)$ and Fermi surface are, respectively, drawn using 40×40 and 200×200 meshes.

closed Fermi surface, whereas the experiment suggests an open Fermi surface in the k_c direction. The difference in Fermi surface comes from the energy of the upper band at the Z point in the Brillouin zone $E(0, c^*/2)$, which is given by the following equation:

$$E_Z = -2t_c + |t_{a1} + t_{a2} - t_{p1} - t_{p2}| \approx 2(|t_a| - t_c). \quad [3]$$

In the case of theoretical calculation, E_Z is slightly lower ($E_Z - E_F = -0.8$ meV) than the Fermi energy, which brings about the closed Fermi surface. Since the theoretical calculation overestimates $t_c(>0)$ or underestimates t_a, E_Z of the actual compound is higher than that of the theoretical calculation ($E_Z - E_F = 48.8$ meV). Since E_Z is close to the Fermi energy E_F, the small difference in transfer integrals makes a big influence on the shape of the Fermi surface near the Z point as shown in Fig. 3. The energy difference between upper and lower bands at Γ point gives the bandwidth $W = 2|t_{a1} + t_{a2} + t_{p1} + t_{p2}| = 0.92$ eV. As shown in Table 2, the bandwidth of (EO-TTP)$_2$AsF$_6$ is slightly smaller than that of isostructural (BDT-TTP)$_2$SbF$_6$. The reduction of the bandwidth is probably ascribed to the non-planar ethylenedioxy group. The bandwidth is comparable to that of (TMTSF)$_2$PF$_6$ (12) and significantly wider than that of β-(BEDT-TTF)$_2$I$_3$ (13). The dimensionality of this compound can be compared with other compounds using the effective mass ratio $m^*_\perp/m^*_{||}$, which spans from 0 in one-dimensional case to 1 in two-dimensional case. As shown in Table 2, the effective mass ratio of (EO-TTP)$_2$AsF$_6$ is 4 times larger than that of (TMTSF)$_2$PF$_6$ which undergoes SDW phase transition, and about half of β-(BEDT-TTF)$_2$I$_3$ which has a closed Fermi surface. This experimental result characterizes the electronic structure of (EO-TTP)$_2$AsF$_6$ among the organic metals with β-type molecular arrangement, and the relatively large inter-stack interaction seems to contribute to the stable metallic property.

TABLE 2
Anisotropic Ratio of Effective Mass and Bandwidth (W)

Compound	$m^*_\perp/m_{||}$	W (eV)	T (K)	Reference
β-(BEDT-TTF)$_2$I$_3$	0.29	0.5	30	13
(EO-TTP)$_2$AsF$_6$	0.15	0.92	300	This work
(BDT-TTP)$_2$SbF$_6$	0.11	1.2	300	10
(BDT-TTP)$_2$AsF$_6$	0.08	1.2	300	10
(TMTSF)$_2$PF$_6$	0.04	1.0	300	12

Figure 4 shows the temperature dependence of $E||a$ and $E\perp a$ reflection spectra from 300 to 12 K. The reflectivity in low-frequency region gradually increases on lowering the temperature, and $E||a$ spectrum is approximately described by the Drude model in this temperature range. However, low-temperature $E\perp a$ spectrum cannot be fitted with a simple Drude model even in the infrared region (15). We analyzed the low-temperature $E||a$ reflectivity using the Drude model assuming that the dielectric constant ε_∞ is temperature independent. In the case of (BDT-TTP)S_bF$_6$, the inter-stack transfer integrals are nearly temperature independent (10). Assuming that the transfer integral t_c at room temperature is temperature independent, we obtained the temperature dependence of t_a, which is shown in the inset of Fig. 4a. The transfer integral increases by about

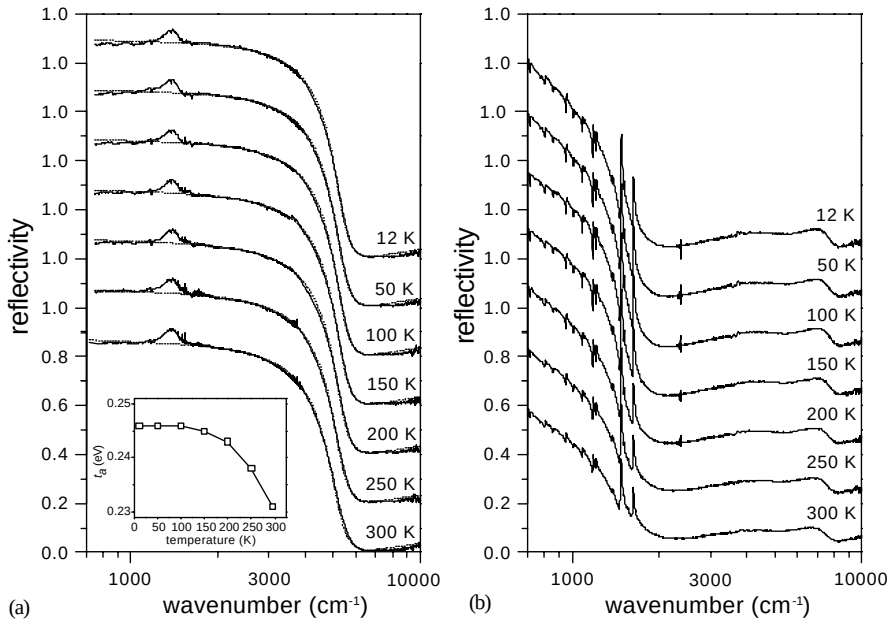

FIG. 4. Temperature dependence of the reflectivity polarized (a) parallel and (b) perpendicular to the a-axis. The dotted line in (a) denotes the reflectivity by the Drude model. The inset of (a) shows the temperature dependence of the intra-stack transfer integral t_a.

10% at 12 K along the stacking direction. Therefore, the dimensionality will decrease slightly at low temperatures. The same tendency was found also in (BDT-TTP)$_2$ SbF_6 (10).

3.2. Electron-Electron Interaction

In the actual materials, the effective mass m^* and the relaxation rate γ depend upon the photon frequency owing to the electron–phonon and electron–electron interactions. We analyzed the frequency dependence in E||a spectra using the following generalized Drude formula (16, 17):

$$\varepsilon(\omega) = \varepsilon_\infty - \frac{\omega_p^*(\omega)}{\omega(\omega + i\gamma(\omega))}, \qquad [4]$$

where the frequency-dependent plasma frequency is given by $\omega_p^*(\omega) = ne^2/\varepsilon_0 m^*(\omega)$. We first calculate the real and imaginary parts of the dielectric function through Kramers–Kronig transformation. The low-frequency region (0–750 cm^{-1}) of the reflectivity was extrapolated by Hagen–Rubens model, and the high-frequency region was approximated by the room-temperature reflectivity curve. The frequency-dependent effective mass $m^*(\omega)$ and relaxation rate $\gamma(\omega)$ is obtained by solving the real and imaginary parts of Eq. (4) at each frequency assuming that $\varepsilon = 2.5$ is temperature independent (see Ref. (17)). The results at 300 and 12 K are shown in Fig. 5. The structure at 0.2 eV comes from the hump in the $E||a$ reflectivity which is derived from the electron-molecular-vibration (EMV) coupling. Neglecting this region, the frequency dependence of the effective mass is very small up to 0.8 eV especially at

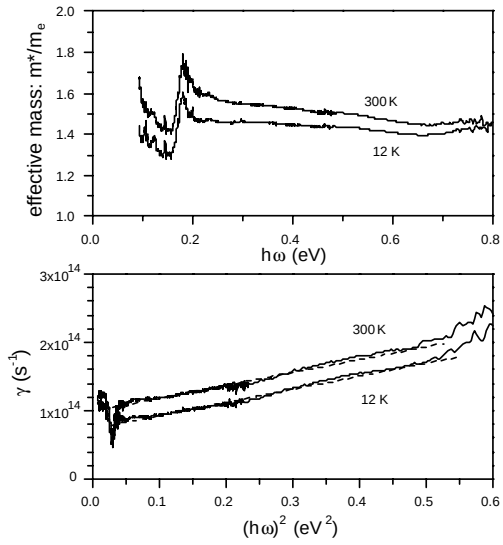

FIG. 5. Frequency dependence of the effective mass $m^*(\omega)$ and relaxation rate $\gamma(\omega)$ at room temperature and 12 K.

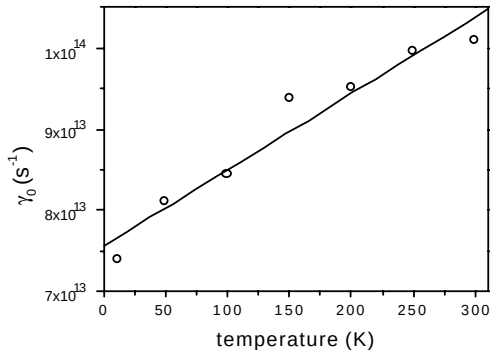

FIG. 6. Temperature dependence of $\gamma_0(T)$, which is obtained by the extrapolation of the high-frequency region using $\gamma\omega = \gamma + b\omega^2$.

12 K. This result is equivalent to the good approximation of Drude model for this compound.

The relaxation rate plotted against the square of photon energy exhibits a straight line as shown in Fig. 5b. This frequency dependence is described by the equation $\gamma(\omega, T) = \gamma_0(T) + b(T)\omega^2$, which is observed in alkali metals and noble metals (18, 19). The parameters obtained by least-squares fitting are $\gamma_0 = 1 \times 10^{14}\,\mathrm{s}^{-1}$, $b = 2 \times 10^{14}\,\mathrm{s}^{-1}\,\mathrm{eV}^{-2}$ for 300 K and $\gamma_0 = 0.7 \times 10^{14}\,\mathrm{s}^{-1}$, $b = 2 \times 10^{14}\,\mathrm{s}^{-1}\,\mathrm{eV}^{-2}$ for 12 K. These values are comparable with $\gamma_0 = 4.6 \times 10^{13}\,\mathrm{s}^{-1}$, $b = 2.4 \times 10^{13}\,\mathrm{s}^{-1}\,\mathrm{eV}^{-2}$ for Au at 295 K. The scattering mechanism of the conduction electron is understood based on the electron-phonon interaction in the same way as the weakly correlated metal (18). The relaxation rate follows the relation $\gamma(\omega, T) = \gamma_0(T) + b(T)\omega^2$ in the temperature range 12–300 K. As shown in Fig. 6, γ_0 decreases at low temperature with the slope of $\sim 1 \times 10^{11}\,\mathrm{s}^{-1}\,\mathrm{K}^{-1}$. From the Drude model, the dc conductivity is given as $\sigma(0) = \varepsilon_0\omega_p^2/\gamma$. If we replace γ by γ_0 in this equation, $\sigma(0)$ is calculated to be 400 S cm^{-1} at room temperature, which agrees well with the dc conductivity value $\sigma_{dc}(RT) = 600\,\mathrm{S\,cm}^{-1}$ (9). However, the low-temperature conductivity $\sigma(0)$ disagrees with σ_{dc}. For example, the ratio $\sigma_{dc}(T)/\sigma(0,T)$ increases from ~ 1 at 300 K to 10–20 at 12 K (9). It is known that the scattering rate γ_0 obtained by the extrapolation of the high-frequency region ($\omega \gg \gamma$) no longer agrees with the scattering rate of dc conductivity at low temperature (18). At low temperature, in other words, $\gamma(\omega) = \gamma_0 + b\omega^2$ does not hold in the low-frequency region in this compound as well. The property in the spectral region higher than 750 cm^{-1} appears to resemble the property of a weakly correlated metal with electron–phonon interaction, which is exceptional in organic conductors. This result suggests weak electron–electron interaction, which is consistent with the small on-site Coulomb energy speculated from the extended π conjugation in EO-TTP. However, the reflectivity in $E \perp a$ polarization is non-Drude like. The reflectivity in the

far-infrared region will present further information on the electron–electron interaction.

4. CONCLUSION

The intra- and inter-stack transfer integrals were determined through the analysis of the polarized reflection spectra. The set of experimentally determined transfer integrals suggested an open Fermi surface contrary to the theoretical prediction. However, the inter-stack interaction of $(EO\text{-}TTP)_2AsF_6$ is much larger than that of the typical quasi-one-dimensional organic metal $(TMTSF)_2PF_6$. The frequency dependence of the relaxation rate of conduction electron in the frequency range 1800–5500 cm^{-1} conformed to the same relation as alkali metals and noble metals, which suggests a weak electron–electron interaction.

ACKNOWLEDGMENTS

K.Y. was supported in part by a Grant-in-Aid for Scientific Research on Priority Areas (B) of Molecular Conductors and Magnets (Area No. 730/Grant No.11224212) from the Ministry of Education, Culture, Sports, Science, and Technology of Japan.

REFERENCES

1. Y. Misaki, H. Fujiwara, T. Yamabe, T. Mori, and S. Tanaka, *Chem. Lett*. 1653 (1994).
2. T. Mori, Y. Misaki, H. Fujiwara, and T. Yamabe, *Bull. Chem. Soc. Jpn*. **67,** 2685 (1994).
3. T. Mori, T. Kawamoto, Y. Misaki, K. Kawakami, H. Fujiwara, T. Yamabe, H. Mori, and S. Tanaka, *Mol. Cryst. Liq. Cryst*. **284,** 271 (1996).
4. T. Mori, T. Kawamoto, Y. Misaki, K. Kawakami, H. Fujiwara, T. Yamabe, H. Mori, and S. Tanaka, *Mol. Cryst. Liq. Cryst*. **284,** 271 (1996).
5. Y. Misaki, N. Higuchi, T. Ohta, H. Fujiwara, T. Yamabe, T. Mori, H. Mori, and S. Tanaka, *Mol. Cryst. Liq. Cryst*. **284,** 27 (1996).
6. T. Mori, Y. Misaki, T. Yamabe, and H. Mori, S. Tanaka, *Chem. Lett*. 549 (1995).
7. T. Mori, H. Inokuchi, Y. Misaki, H. Nishikawa, T. Yamabe, H. Mori, and S. Tanaka, *Chem. Lett*. 2085 (1993).
8. T. Mori, H. Inokuchi, Y. Misaki, H. Nishikawa, T. Yamabe, H. Mori, S. Tanaka, *Chem. Lett*. 733 (1993).
9. Y. Misaki, K. Tanaka, M. Taniguchi, T. Yamabe, T. Kawamoto, T. Mori, *Chem. Lett*. 1249 (1999).
10. J. Ouyang, K. Yakushi, Y. Misaki, and K. Tanaka, *J. Phys. Soc. Jpn*. **67,** 3191 (1998).
11. C. S. Jacobsen, D. B. Tanner, and K. Bechgaard, *Phys. Rev. Lett*. **46,** 1142 (1981).
12. C. S. Jacobsen, D. B. Tanner, and K. Bechgaard, *Phys. Rev. B* **28,** 7019 (1983).
13. H. Tajima, K. Yakushi, H. Kuroda, and G. Saito, *Solid State Commun*. **561,** 59 (1985).
14. The transfer integrals are estimated assuming $t = -10$ S eV.
15. On lowering the temperature, the low-frequency reflectivity increases, but the reflectivity minimum in high-frequency region does not decrease. Therefore, both the high- and low-frequency regions of reflectivity are incompatible with Drude model.
16. F. Cao, D. B. Romero, and D. B. Tanner, *Phys. Rev. B* **47,** 1036 (1993).
17. S. Kimura, T. Nanba, S. Kunii, and T. Kasuya, *Phys. Rev. B* **50,** 1406 (1994).
18. J. B. Smith, and H. Ehrenreich, *Phys. Rev. B* **25,** 923 (1982).
19. G. R. Parkins, W. E. Lawrence, and R. W. Christy, *Phys. Rev. B* **23,** 6408 (1981).